Effective release rates at single rat Schaffer collateral–CA1 synapses during sustained theta-burst activity revealed by optical imaging

G. B. Awatramani, J. D. Boyd, K. R. Delaney and T. H. Murphy

J. Physiol. 2007;582;583-595; originally published online Apr 26, 2007;

DOI: 10.1113/jphysiol.2007.130286

Effective release rates at single rat Schaffer collateral–CA1 synapses during sustained theta-burst activity revealed by optical imaging

G. B. Awatramani[1], J. D. Boyd[2], K. R. Delaney[2] and T. H. Murphy[1]

[1] *University of British Columbia, 2255 Wesbrook Mall, Vancouver, British Columbia, Canada V6T 1Z3*
[2] *Department of Biology, Box 3020 Stn CSC, University of Victoria, Victoria, British Columbia, Canada V8W 3N5*

To understand how information is coded at single hippocampal synapses during high-frequency activity, we imaged NMDA receptor-mediated Ca^{2+} responses in spines of CA1 neurons using two-photon microscopy. Although discrete quantal events were not readily apparent during continuous theta-burst stimulation (TBS), we found that the steady-state dendritic Ca^{2+} response was spatially restricted (half-width $< 1\ \mu$m), voltage dependent and sensitive to MK-801, indicating that that it was mediated by activation of NMDA receptors at single synapses. Partial antagonism of NMDA receptors caused a similar reduction of NMDA EPSCs (measured at the soma) and local dendritic Ca^{2+} signals, suggesting that, like EPSCs, the steady-state Ca^{2+} signal was made up of a linear addition of quantal events. Statistical analyses of the steady-response suggested that the quantal size did not change dramatically during TBS. Deconvolution of TBS-evoked Ca^{2+} responses revealed a heterogeneous population of synapses differing in their capacity to signal high-frequency information, with an average effective steady-state release rate of $\sim$2.6 vesicles synapse^{-1} s^{-1}. To assess how the optically determined release rates compare with population measures we analysed the rate of decay of peak EPSCs during train stimulation. From these studies, we estimated a unitary vesicular replenishment rate of 0.02 s^{-1}, which corresponds to an average release rate of $\sim$0.8–2 vesicles s^{-1} at individual synapses. Additionally, extracellular recordings from single Schaffer collaterals revealed that spikes propagate reliably during TBS. Hence, during high-frequency activity, Schaffer collaterals conduct spikes with high fidelity, but release quanta with relatively lower efficiency, leaving NMDA receptor function largely intact and synapse specific. Heterogeneity in release rates between synapses suggests that similar patterns of presynaptic action potentials could trigger different forms of plasticity at individual synapses.

(Received 13 February 2007; accepted after revision 25 April 2007; first published online 26 April 2007)
Corresponding author T. H. Murphy: 2255 Wesbrook Mall, Vancouver, British Columbia, Canada V6T 1Z3.
Email : thmurphy@interchange.ubc.ca

Synaptic information transfer becomes independent of the frequency of presynaptic activity when the 'readily releasable pool' (RRP) of docked synaptic vesicles is exhausted during periods of sustained activity. Under these conditions transmission is limited by the vesicle replenishment rate (Elmqvist & Quastel, 1965; Abbott *et al.* 1997; Harata *et al.* 2001). This rate is determined by the time it takes fresh quanta to refill the RRP and become release-ready. Consequently, after the RRP has been depleted, postsynaptic responses measured during sustained activity can be used to estimate the vesicle replenishment rate at a synapse (Elmqvist & Quastel, 1965; Wesseling & Lo, 2002). Traditionally, the decay and the relative steady-state profiles of compound electrophysiological responses were used to assess the average replenishment rate at synapses (Elmqvist & Quastel, 1965). However, activity-dependent conduction failure in presynaptic axons (Soleng *et al.* 2004) and heterogeneity in the release properties between synapses (Murthy *et al.* 1997; Rosenmund *et al.* 2002) can prevent straightforward interpretation of these results (Brody & Yue, 2000; Debanne, 2004). Some of these limitations were circumvented when optical tools were used to probe activity at single presynaptic boutons in cultured preparations (Sankaranarayanan & Ryan, 2000; Sara *et al.* 2002). However, due to the relatively weak optical signal produced by the release of single vesicles, estimates of steady-state vesicle replenishment rates were derived from an averaged response from a number of boutons

This paper has online supplemental material.

DOI: 10.1113/jphysiol.2007.130286

(Sankaranarayanan & Ryan, 2000; Sara *et al.* 2002). Therefore, direct measurement of the rate at which individual hippocampal synapses operate during sustained stimulation has not been possible. Furthermore, little is known about how presynaptic release is transformed into postsynaptic signals during sustained activity (Zhou *et al.* 2000).

The processing of vesicle release by postsynaptic NMDA receptors during TBS is also particularly interesting because the temporal patterns by which these receptors are activated can initiate various forms of long-term synaptic plasticity (Dudek & Bear, 1992). The NMDA receptor is a point of convergence for a number of modulatory pathways (Kotecha & MacDonald, 2003), and may be subject to regulation during tonic stimulation (Morishita *et al.* 2005). Thus, in addition to understanding how presynaptic action potentials are transformed into released quanta, insight into how postsynaptic NMDA receptors signal during high-frequency synaptic activity has important implications for processes that govern long-term plasticity.

Here, we measure the response properties of both the pre- and postsynaptic elements of single synapses to sustained TBS. To monitor vesicle release at single synapses, NMDA receptor-mediated Ca^{2+} influx at post-synaptic sites (Muller & Connor, 1991; Murphy *et al.* 1994*a*; Yuste & Denk, 1995; Emptage *et al.* 1999; Oertner *et al.* 2002) was measured using two-photon laser scanning microscopy. These Ca^{2+} responses depend on both a vesicle being released and its postsynaptic detection, and thus provide a read-out of the 'effective' release rate. Statistical and deconvolution analysis of the Ca^{2+} responses to sustained TBS provide new insights into how single quanta are processed by postsynaptic NMDA receptors and the steady-state rate at which vesicles are released at single synapses.

Methods

Acute hippocampal slices (250–300 μm) were prepared from P16- to P22-day-old rats that were killed by decapitation under deep halothane anaesthesia (single dose administered by ether jar) consistent with Canadian Council on Animal Care use guidelines. Slices were perfused with ACSF containing (mM): 125 NaCl, 25 glucose, 2.5 KCl, 1 $MgCl_2$, 2 $CaCl_2$, 1.25 NaH_2PO_4 and 25 $NaHCO_3$, bubbled with 5% CO_2–95% O_2 at 35°C. All electrophysiological recordings were performed using a MultiClamp 700A or Axopatch 200B (Molecular Devices) amplifier. Signals were filtered at 5 kHz and sampled at 20 kHz using pCLAMP 9.0 (Molecular Devices).

Extracellular recordings

'Loose patch' extracellular potentials from single axons in the CA1 area of stratum radiatum were made as previously described (Raastad & Shepherd, 2003). These recordings most probably represented activity of the Schaffer collaterals, since these are most abundant in this region. In addition, the stimulating electrode was placed ~0.5 mm away from the site of recording to further minimize the chance of recording from axons of local inhibitory neurons.

Patch-clamp recordings

Whole-cell recordings from hippocampal CA1 pyramidal cells were made with patch electrodes (2–3 MΩ) containing (mM): 140 $CsMeSO_3$, 1 $MgCl_2$, 10 Hepes, 2 ATP, 0.3 GTP, 10 phosphocreatine, 1 mM Fluo 5F (~320 mosmol l^{-1}) and pH adjusted to 7.3 with CsOH. QX314 (2 mM) was added to the internal solution to block Na^+ channels to improve the space clamp. After dye equilibration (~30 min), the cell of interest was voltage-clamped near 0 mV to relieve the Mg^{2+} block of NMDA receptors and to inactivate voltage-dependent Ca^{2+} channels. In some cases, as indicated, cells were held at −20 mV to provide some driving force for observation of NMDAR activity. Under these conditions, Ca^{2+} influx through NMDA receptors is maximized and serves as a faithful measure of glutamate in the synaptic cleft. An ACSF-filled stimulating electrode was placed ~150 μm away from the recorded cell, and its position optimized until synapses showing robust Ca^{2+} responses to low-frequency (0.1 Hz) stimulation were identified. The intensity of the stimulus (2–40 V, 50–100 μs) in the imaging experiments was set to 25–50% above threshold to prevent presynaptic conduction failure during train stimulation. Errors are reported as ± S.E.M.

Image acquisition

Two-photon fluorescence excitation was performed with a Coherent (Santa Clara, CA, USA) Mira 900 Ti–sapphire laser (pumped by a 5 W Verdi laser), tuned to 810 nm to excite Fluo 5F. Images were obtained through an Olympus (Tokyo, Japan) IR-LUMPlanFl water-immersion objective (60×; 0.9 numerical aperture) and captured using custom software routines (IgorPro; Wavemetrics, Eugene, OR, USA) at 10–20 Hz, with a pixel size of ~0.12 μm. During low-frequency stimulation, 15 frames (~1.5 s) were captured. During TBS, 50 frames (~5 s) were acquired with 10 s intervals. The laser power was minimized (5–15 mW at the objective back aperture) to prevent excessive bleaching and photodamage.

Image analysis

Baseline fluorescence (F_0) was determined by averaging fluorescence 0.5–4 s before the onset of the stimuli

(shorter baselines were measured during low-frequency stimulation). Aside from the subtraction of the dark current of the photomultiplier tube, no other background correction was performed. F_{max} was determined by measuring fluorescence during trains of antidromic stimulation at the end of the experiment, and was > 8- to 10-fold above resting fluorescent levels. Ca^{2+} signals are presented as relative change normalized to the resting fluorescence and were computed as:

$$(\Delta F/F_0)(t) = (F(t) - F_0)/F_0$$

Statistical and deconvolution analysis

Assuming that the variance of Ca^{2+} signals at steady state was dominated by randomly occurring quantal events that summed linearly, the mean quantal size can be estimated as $2\sigma^2$/mean of the steady-state response (Katz & Miledi, 1972), provided the duration of the elementary signal is brief relative to the interval over which the variance is computed over. The mean (F_{ss}) and variance ($\sigma^2{}_{ss}$) of the steady-state signal was computed over 10–30 s. This time interval is sufficiently long, as the size of the elementary signal could be accurately estimated from the fluctuations in simulated Poisson trains, which had randomly distributed quantal events with similar characteristics as those measured during low frequency stimulation (LFS) (Fig. 5B). The $\sigma^2{}_{Fss}$ was corrected for baseline variance composed of dark noise, shot noise and changes in resting Ca^{2+}. The quantal size estimate (QSE) was computed as:

$$\mathrm{QSE} = 2\left(\sigma_{ss}^2\right)/F_{ss}$$

Deconvolution of the train response with an idealized quantal event was performed as previously described (Van der Kloot, 1988; Diamond & Jahr, 1995). Briefly, the averaged quantal response was fitted by the difference of exponential functions:

$$Ae^{(-x/\tau_r)} - e^{(-x/\tau_d)}$$

where A is the amplitude of the quantal event, τ_r and τ_d are the rise and decay time constants of the quantal response, respectively (Fig. 5*Aa*). Discrete Fourier transforms of the idealized quantal responses were divided by the Fourier transforms of the responses to train stimuli. The result was inverse Fourier transformed to produce the release rate histogram in the time domain. The amplitudes of release rates obtained from the deconvolution analysis were set to a threshold to create rasters of discrete instantaneous release rates (0, 1 or 2 quanta per 100 ms bin; Figs 5 A*b* and 6*B*). The thresholds were optimized to minimize differences in sum of square errors (SSE) between the actual TBS-evoked Ca^{2+} response and a 'model' train response, which was obtained by summing quantal responses according to the computed discrete release rates derived from deconvolution analysis.

Results

LFS- and TBS-evoked Ca^{2+} responses at single synapses

To understand how the release machinery of small synapses copes with prolonged high-frequency information, we first monitored activity at single synapses by imaging spines and dendrites of CA1 pyramidal neurons. Since most spines are contacted by single presynaptic boutons that under most circumstances release one vesicle per action potential (Stevens & Wang, 1995; Prange & Murphy, 1999; Hanse & Gustafsson, 2001; Oertner *et al.* 2002), but see (Wadiche & Jahr, 2001), optical 'quantal' properties could be estimated by imaging NMDA receptor-mediated Ca^{2+} transients at single postsynaptic sites, in response to low frequency stimulation (LFS) (0.1 Hz) of the Schaffer collaterals (Yuste & Denk, 1995; Oertner *et al.* 2002; Sabatini *et al.* 2002). Neurons loaded with fluorescent Ca^{2+} indicator (1 mM Fluo 5F; Fig. 1*A*) were voltage clamped at ~0 mV to relieve the Mg^{2+} block of NMDA receptors and to inactivate voltage-dependent Ca^{2+} channels. Under these conditions, vesicular release from the presynaptic bouton could be detected as a postsynaptic quantal Ca^{2+} signal. An example of such a measurement is illustrated in Fig. 1*B*. LFS evoked changes in spine fluorescence that was time-locked to

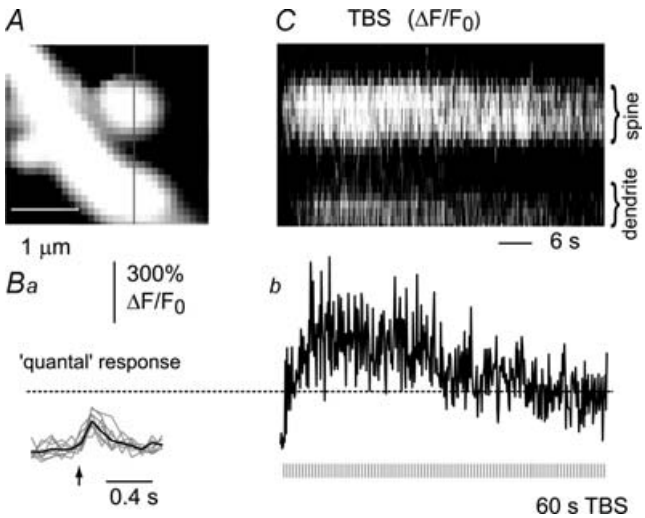

Figure 1. Single spine Ca^{2+} responses to LFS and TBS
A, an image of a spine and dendrite. *B*, the relative intensity ($\Delta F/F_0$) of the responses in the spine during: (*a*) LFS (superimposed grey traces are single trials and the black trace is the average quantal response, 0.1 Hz) and (*b*) continuous TBS (4 pulses at 50 Hz given every 200 ms). The vertical arrow in *Ba* indicates the time of stimulation. The steady-state amplitude of the TBS-evoked Ca^{2+} responses is indicated by the horizontal dotted line. *C*, the $\Delta F/F_0$ along the vertical grey line in *A* is plotted as a function of space and time during continuous TBS.

the stimulus (Fig. 1*Ba*, grey traces). The average quantal properties of the synapse were then estimated by averaging the Ca^{2+} transients of the successful events (Fig. 1*Ba*, black trace). Single quanta caused a $76 \pm 53\%$ $\Delta F/F_0$, which decayed to baseline with an exponential time constant of 287 ± 100 ms ($n = 16$).

After the quantal parameters were determined using LFS, the synapse was subjected to a 60 s train of TBS (1200 stimuli; Fig. 1*Bb* and *C*). To ensure reliable presynaptic stimulation, stimulus intensity was set > 25% above response threshold (see Fig. 7 for reliability of spike activation). At the onset of the train when release was highest, Ca^{2+}-induced fluorescence rose in the spine as well as in the dendritic shaft (Fig. 1*C*), making it difficult to confirm that the signal originated from the spine of interest. The initial optical response to the onset of train stimulation was thus omitted from further analysis. After ~5–30 s of stimulation, the Ca^{2+} response reached a lower steady-state level (Fig. 1*Bb*) (Otsu & Murphy, 2004) and was higher in the spine than in the parent dendrite. However, individual quantal-like events (Fig. 1*Bb*) were not easily distinguishable in the spine during the train stimulation. Figure 1*C* plots the relative fluorescence change ($\Delta F/F_0$) along the vertical grey line that crosses the spine head and the parent dendrite (shown in Fig. 1*A*) during TBS. We next determined whether this fluctuating sustained Ca^{2+} signal in the spine was caused by the repeated activation of NMDA receptors by continuous stochastic vesicular release during the long TBS, or by Ca^{2+} elevation from a non-NMDA receptor-dependent source.

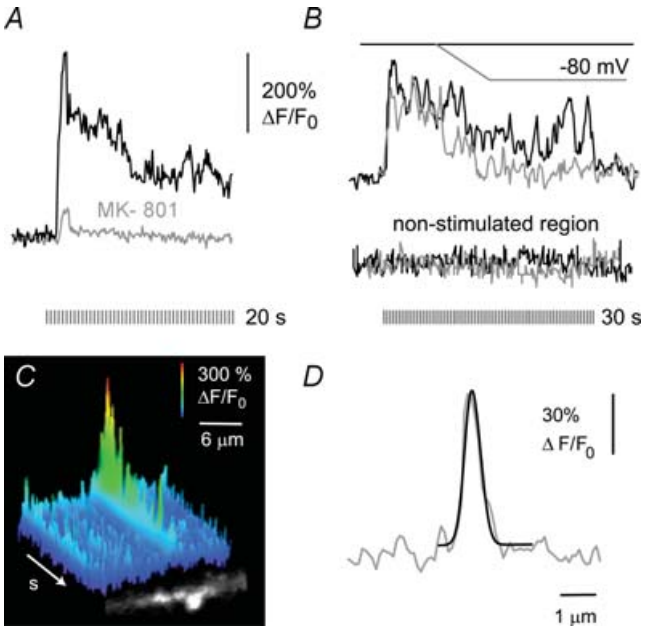

Figure 2. Ca^{2+} responses at steady-state are mediated by NMDA receptors and are spatially restricted
A, Ca^{2+} response from a spine in the absence (black trace) and presence of 10 μM MK-801 (grey trace). *B*, Ca^{2+} responses measured at +10 mV (black trace) and during a voltage ramp to −80 mV (grey trace). *C*, spatio-temporal Ca^{2+} profile along the dendrite during continuous TBS (diagonal arrow 10 s). *D*, the average spatial Ca^{2+} profile during the steady-state response was estimated by fitting it to a Gaussian function (black line).

Steady-state Ca^{2+} responses are mediated by NMDA receptors and are spatially restricted

Two pieces of experimental data suggested that the plateau Ca^{2+} response evoked by TBS was mediated by repeated synaptic activation of NMDA receptors. First, the application of the use-dependent NMDA receptor antagonist MK-801 (10 μM) completely blocked the sustained phase of the train response (Fig. 2*A*; $96 \pm 3\%$ inhibition; $n = 5$). These data demonstrate that responses were mediated by NMDA receptors and not direct electrical stimulation of the dendrite. Moreover, the flat response observed during trials with MK-801 demonstrated that the dye did not undergo a significant degree of bleaching under our imaging conditions. Note, although the fluorescence intensity (indicative of Ca^{2+}-bound dye) is relatively low in MK-801, the rate of bleaching is expected to be independent of amount of fluorophore. Second, hyperpolarizing the membrane potential to −80 mV after the peak response had occurred led to a loss in steady-state response at the site of interest ($93 \pm 5\%$ inhibition; $n = 5$; Fig. 2*B*), consistent with the rapid induction of Mg^{2+} block of active NMDA receptors at these potentials. During hyperpolarization, no time- or voltage-dependent changes in basal fluorescence were observed in neighbouring non-stimulated sites, suggesting that voltage-gated Ca^{2+} channels were largely inactivated at 0 mV. Collectively, these data suggest that responses to continuous TBS are mediated by synaptically activated NMDA receptors.

To verify that the optical signal originated from the activation of single synapses, and not from diffusion of Ca^{2+} from neighbouring sites, the spatio-temporal profile of Ca^{2+} was measured in the parent dendrites during the steady-state TBS response. The $\Delta F/F_0$ along the dendrite was plotted as a function of space and time (Fig. 2*C*). Once synaptic depression ensued, Ca^{2+} gradients associated with quantal events were extremely restricted (Fig. 2*D*), with a full-width at half-maximum (FWHM) spread of 0.66 ± 0.51 μm ($n = 16$), consistent with these signals arising from the activation of single synapses. Thus, during intense ongoing activity, TBS-evoked Ca^{2+} signals remain synapse specific.

Near-linear addition of quantal events give rise to steady-state Ca^{2+} response

Our data are consistent with the steady-state Ca^{2+} signal being maintained by stochastic release of single vesicles

(Fig. 2). It is conceivable that a variety of non-linear dynamic processes could potentially contribute to the steady-state Ca^{2+} response. However, we minimized potential non-linearities by using a high concentration of Ca^{2+} indicator (1 mM Fluo 5F) and analysing only steady-state responses. The large added buffer capacity for Ca^{2+} provided by the fluorophore also severely limits the amplitude of quantal Ca^{2+} transients (Oertner *et al.* 2002; Sabatini *et al.* 2002), and thus signals initiated by multiple vesicles add relatively linearly (Oertner *et al.* 2002). Moreover, limiting the level of Ca^{2+} elevation also reduces non-linear changes in down-stream Ca^{2+}-sensitive processes such as NMDA receptor function and Ca^{2+} extrusion (Morishita *et al.* 2005; Scheuss *et al.* 2006; Sobczyk & Svoboda, 2007). To determine whether the level of the steady-state response was directly proportional to release we asked whether these quantal events added linearly?

To experimentally verify that quantal Ca^{2+} signals added linearly to produce the steady-state response, we examined the effects of partially antagonizing NMDA receptors (using 1.5 μM AP5) on the local synaptic Ca^{2+} signals *versus* EPSCs measured in the soma. Blocking a certain fraction of NMDA receptors should cause a linear decrease in the TBS-evoked EPSCs. If non-linear processes such as indicator saturation or changes in extrusion occurred during steady-state Ca^{2+} response, then blocking a known fraction of receptors would not cause a similar decrease in the fluorescent signal. However, we found that the NMDA receptor-mediated Ca^{2+} signals and EPSCs were reduced by a similar fraction by low concentrations of AP5 (Fig. 3). Figure 3*A* shows an example of train-evoked Ca^{2+} responses in a dendritic spine (Fig. 3*Aa*) and the simultaneously recorded somatic EPSCs (in the presence of GABA and AMPA receptor antagonists). After a 20 min bath application of AP5 (long durations were required

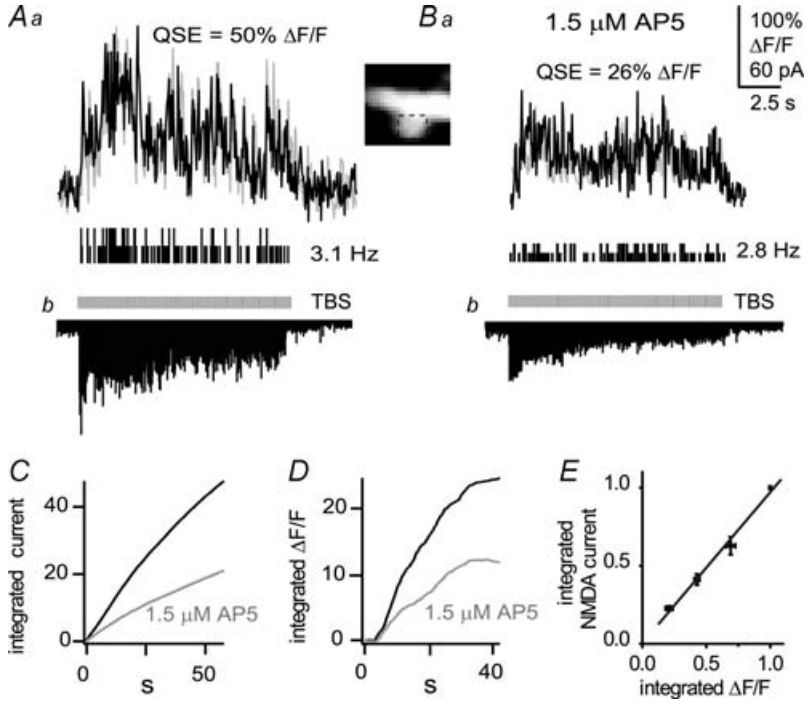

Figure 3. Dendritic Ca^{2+} signals are linearly related to NMDA EPSC
A, the simultaneous measurement of NMDA receptor-mediated Ca^{2+} response in a single spine (illustrated on the right; the region of interest is depicted by the dashed black box 0.9 μm in width) (*a*) and somatic NMDA receptor-mediated EPSCs ($V_{hold} = -20$ mV) evoked by TBS (*b*). A raster of the instantaneous release rate estimated by deconvolving the TBS-evoked response with the fitted quantal response (peak amplitude 50% $\Delta F/F$; inset; also see Fig. 4 and results for details). *Ba*, Ca^{2+} responses and, *b*, EPSCs evoked by the same stimulus, in the presence of subsaturating NMDA receptor antagonist AP5. The raster of the instantaneous release rate was estimated by deconvolving the TBS-evoked response with a quantum of similar kinetics, but with a peak amplitude of 26% $\Delta F/F$ (the height of the raster is also reduced to half the amplitude highlight this reduction). The steady-state release rate is noted besides the raster plots in *A* and *B*. The grey trace in *Aa* and *Ba* is the model train constructed by adding quanta according to the estimated release rate. The integral of the peak NMDA EPSC (*C*) and Ca^{2+} during the course of TBS (*D*). *E*, a plot of the relative integrated EPSC *versus* integrated Ca^{2+} signals during graded levels of AP5 block of NMDARs. Integrals were normalized to values in control conditions. Different levels of antagonism were achieved by varying the concentration of AP5 (1–5 μM; $n = 6$ cells).

to ensure that the drug equilibrated evenly throughout the slice and antagonized all synapses equally), both spine Ca^{2+} and the EPSCs (Fig. 3*B*) were reduced. To quantify the amount of block achieved, we integrated the peak currents (Fig. 3*C*) and Ca^{2+} signal (Fig. 3*D*) over the duration of the train stimulus and found that they were reduced by 56% and 63%, respectively. In similar experiments utilizing different concentrations of AP5 (1–5 μM) to achieve graded levels of NMDA receptor antagonism also revealed a linear relationship between integrated EPSCs and Ca^{2+} signals evoked by TBS (Fig. 3*E*). Data from six cells were normalized to control levels and then pooled together. The current *versus* Ca^{2+} signals measured during graded NMDA receptor blockade fitted well to a straight line with a slope of 0.96 ($r^2 = 0.98$; $P < 0.005$; Fig. 3*E*). The finding that Ca^{2+} signals and EPSCs are linearly related strongly suggests that the steady-state portion of the Ca^{2+} transient during train stimulation is made up of a near-linear addition of quantal events.

Statistical and deconvolution analysis of steady-state Ca^{2+} responses

NMDA receptors are known to be the target of a multitude of regulatory pathways and it was possible that down-modulation of these receptors (Morishita *et al.* 2005; Sobczyk & Svoboda, 2007) contributed to synaptic depression observed optically. Assuming that sustained TBS-evoked Ca^{2+} response was made up by a near-linear addition of single quantal events (Fig. 3), we sought to estimate the quantal size from fluctuations in the sustained phase of the Ca^{2+} signal (Katz & Miledi, 1972) (see Methods). Non-stationary release properties or large variations in quantal amplitudes at a synapse could prevent a clear-cut interpretation of the results (Haller *et al.* 1998). Nonetheless, we observed that the quantal sizes estimated from the variance-to-mean ratio ($\Delta F/F_0 = 71 \pm 57\%$) was remarkably similar to that observed during LFS, which is expected to cause the release of single quanta ($\Delta F/F_0 = 76 \pm 53\%$, $n = 12$; $P = 0.85$; Fig. 4*B*). Thus, under our experimental conditions, NMDA receptors appear to be functional and relatively unchanged during periods of heavy use.

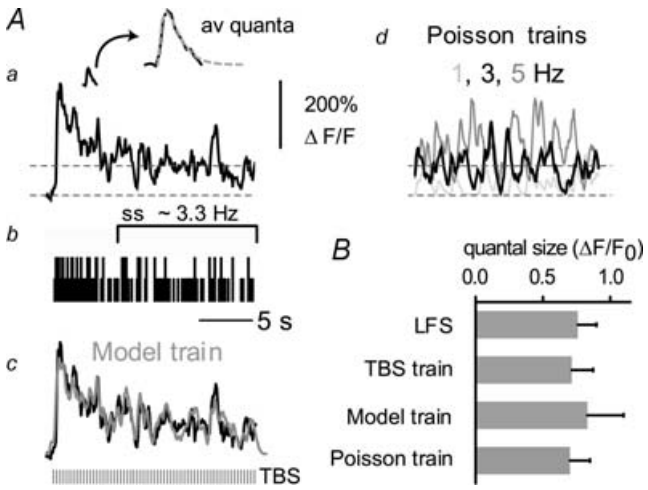

Figure 4. Release rate estimated by deconvolution analysis
Aa, the TBS-evoked Ca^{2+} response at a single synapse (from Fig. 2*C*) decays to a steady state indicated by the horizontal dashed line. The average quantal response evoked during LFS is shown on the same scale as *a*, or at 5× (right; insets). The dashed grey line represents a double exponential fit: $A\ (e^{(-x/\tau rise)} - e^{(-x/\tau decay)})$ of the quantal response. *Ab*, raster of the instantaneous release rates obtained by deconvolving the TBS-evoked response (*Aa*) with the fitted quantal response (*Aa* inset). *Ac*, a model train (grey trace), constructed by summing the quantal responses according to *Ab*, is compared with the TBS-evoked Ca^{2+} response. *Ad*, 1 Hz (light grey), 3 Hz (black) and 5 Hz (grey) Poisson trains, simulated with the average quantal response are illustrated. The horizontal line marks the mean of the 3 Hz train. *B*, the quantal size estimate (QSE) obtained during LFS, or from the mean-to-variance ratio of the steady-state responses during the real and simulated trains.

Since the TBS-evoked Ca^{2+} signal appeared to be formed by the addition of quanta with a fixed average size, it provides a good measure of vesicle release during TBS. To estimate the instantaneous release rate at individual synapses, we deconvolved the Ca^{2+} response induced by sustained TBS with an idealized quantal response obtained from a fit of the average response to LFS (Fig. 4*Aa* inset; in this example the $\Delta F/F_0$ measurement is from the synapse shown in Fig. 2*C*). The outcome of the deconvolution procedure was set to a threshold to produce discrete release rates (Fig. 4*Ab*; see Methods). The 'noisy' TBS-evoked Ca^{2+} responses were thereby transformed into a raster plot indicating the time points at which vesicles were apparently released.

To assess the validity of the release rate estimates, a model train was constructed by summing the average quantal response at every time point indicated by the raster plot. The simulated train was found to closely follow the measured response ($r^2 = 0.80 \pm 0.09$; $P < 0.0005$; Fig. 4*Ac*). In addition, the quantal sizes estimated from the variance-to-mean ratio of the model train were similar to those of the measured Ca^{2+} signal (Fig. 4*B*). Alternatively, since release events were rare and presumably stochastic during the steady-state phase, we also simulated trains using Poisson-distributed events. The average rate was set to that estimated from the deconvolution analysis. The observed mean and variance of the steady-state optical response at a given synapse was reproduced well by the simulated Poisson train Ca^{2+} responses (Fig. 4*Ad*). Higher and lower rates are shown for comparison (Fig. 4*Ad*). These simulations that are based on random summation of quantal events support our estimates of the steady-state release rates.

To experimentally test the robustness of our analysis procedures we compared the results obtained from Ca^{2+} signals measured before and after partial antagonism of NMDA receptors where quantal size was reduced by a

known percentage (Fig. 3*A* and *B*). The example in Fig. 3 shows that when EPSCs were blocked by ∼50%, the quantal size determined from the variance-to-mean ratio was also decreased by a similar fraction (50 *versus* 26% $\Delta F/F$ in control and AP5, respectively). Yet, even under conditions of reduced signal to noise, deconvolution of the TBS-evoked Ca^{2+} responses yields a similar steady-state release rate to that obtained in control conditions (2.8 *versus* 3.1 Hz; Fig. 3*A* and *B*). Together, these results support the use of the statistical and deconvolution methods used to derive quantal size and release rates at CA1 synapses during trains of stimulation.

Heterogeneity in steady-state release rate amongst individual synapses

Although all synapses responded similarly to the onset of the train stimulation, we found that they differed dramatically in their ability to respond to continuous TBS. Examples of the TBS-induced Ca^{2+} responses from five synapses are illustrated in Fig. 5*Aa*. The corresponding estimated times at which individual quantal events occurred during these trains are indicated in Fig. 5*Ab*. Steady-state release rates were computed by averaging the total number of events in the last 10–20 s of the train response. The distribution of steady-state release rates from 16 synapses (taken from 15 cells) was continuous, but positively skewed toward higher release rates (Fig. 5*B*), with an average rate of 2.6 vesicles s^{-1}. Thus, different synapses within the same class of neuron can be distinguished by their ability to signal high-frequency information during continuous activity.

TBS-evoked AMPA and NMDA receptor-mediated EPSCs

To compare release rates of single synapses derived from direct optical measurements to the population average, we analysed the rate of decay of the peak EPSC amplitudes during train stimulation and then employed the analysis approach previously described (Wesseling & Lo, 2002) and described in Supplementary material available online (see Supplementary analysis/equations). The average release rates (estimated in units of vesicles per synapse) obtained by measuring compound AMPA receptor-mediated EPSCs (in 50 μM AP5), in voltage-clamped CA1 neurons are shown in Fig. 6*A* and *C*. At 35°C, ∼900 presynaptic stimuli were required to drive synapses to a steady-state EPSC current. The fraction of the EPSC response maintained at steady state during the train is determined by the replenishment rate (as well as the rate of presynaptic stimulation). Using previously formulated quantitative methods (Wesseling & Lo, 2002), we estimated the replenishment rate for the data set presented in Fig. 6*B* to be 0.02 s^{-1} (see online Supplementary material). Based on this release rate, the fraction of vesicles in the total recycling pool (TRP) that recover and are subsequently released can be derived from eqn (S3) (see Supplementary material), and is depicted as a dashed grey line in Fig. 6*B*. As expected, at steady state the fraction of the TRP recovered is equal to the relative steady-state amplitude of the EPSC, indicating that the estimate of the replenishment rate is accurate within the constraints of our model. This value for the replenishment rate was derived from a large population of AMPA EPSCs and can then be compared to more direct estimates of release rates determined from subsequent Ca^{2+} imaging of individual synapses (see Discussion).

Due to their faster decay kinetics (reducing event overlap), AMPA receptor-mediated EPSCs were used in the estimation of steady-state release rates. However, train-evoked NMDA receptor-mediated EPSCS also showed a similar behaviour. In response to TBS, the peak amplitude of both AMPA and NMDA EPSCs decayed to a steady-state level ∼25% of the initial response. The average peak AMPA and NMDA EPSC amplitude for each burst is plotted in Fig. 6*D*. At the onset of the

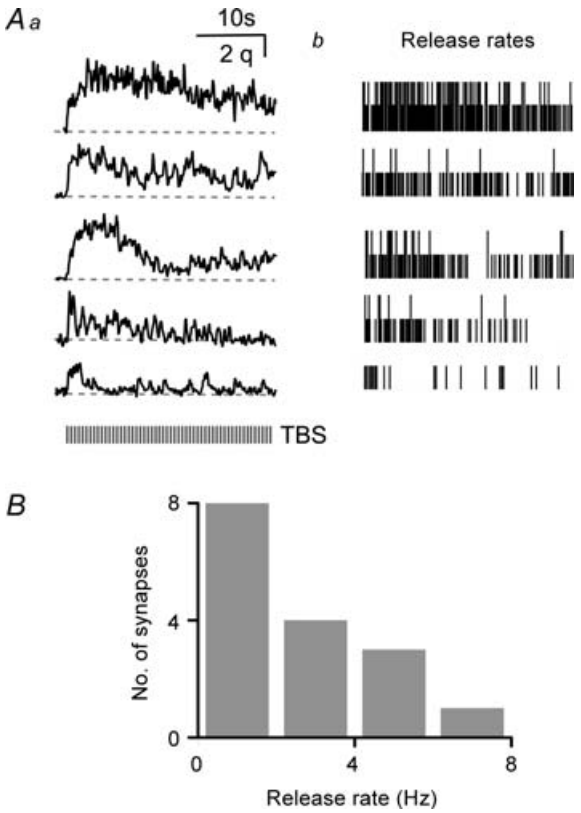

Figure 5. Release rate are heterogeneous between CA3–A1 synapses
Aa, exmples of TBS-evoked Ca^{2+} responses at different spines, normalized to the quantal response measured during LFS (scale bar 2 quanta). *b*, the instantaneous release rates estimated for each synapse shown in *a* are plotted alongside the traces. *B*, a histogram of the mean steady-state release rates obtained from 16 synapses (15 cells).

train there was a small difference in the decay of peak amplitudes of AMPA and NMDA EPSCs. It is not clear if this difference arises from non-linearities in AMPA or NMDA receptor signalling. Since in subsequent imaging experiments we do not analyse the initial response to TBS we did not investigate this difference further. After the first few seconds of stimulation, both AMPA and NMDA EPSCs decayed to steady state with an identical time course ($\tau = 18.3 \pm 0.6$ s ($n = 8$) and 19.3 ± 0.8 s ($n = 6$), respectively). Moreover, repeated presentation of train stimuli evoked similar responses indicating that such stimulation did not cause a significant run-down of the response (Fig. 6*E*). The observation that the peak amplitude of AMPA- and NMDA-mediated EPSCs follow a similar decay time course (~18–19 s) and reach similar steady-state levels during prolonged stimulation, suggests that the locus of depression is largely presynaptic in origin.

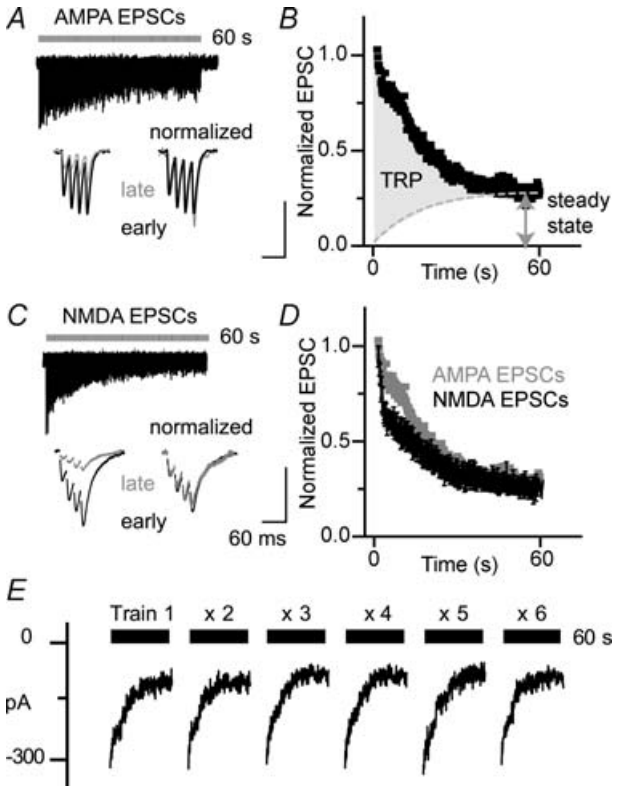

Figure 6. TBS-evoked AMPA and NMDA receptor-mediated EPSCs
A, AMPA EPSCs evoked by 60 s of TBS. Average of first (black) and last (grey) five responses of the train (bottom left), are normalized to the first EPSC in the burst (bottom right). *B*, the average amplitude of each burst is plotted as a function of time ($n = 8$ cells). The fraction of the response that recovers and subsequently undergoes depression during the train (predicted by eqn (S3); see Supplemental information), is indicated by the dashed grey line. The total recycling pool (TRP) is shaded in grey. *C*, NMDA EPSCs evoked by TBS. *D*, the average peak amplitude of AMPA and NMDA receptor components of EPSCs is plotted ($n = 6$ cells). *E*, the EPSC peak amplitude (average of each burst) in response to 6 consecutive trains (60 s TBS) applied at 5 min intervals.

Although electrophysiological recordings only provide an indirect population measurement of the average release rate of synapses, they offer superior temporal resolution of the response profile during train stimuli over a Ca^{2+}-imaging approach. During TBS, the latency of EPSCs increased but responses still remained well locked to the stimulus (Fig. 6*A* and *C*, insets). When normalized to the first EPSC in the burst, averaged AMPA and NMDA EPSCs recorded early and late in the train were not dramatically different in kinetics. This indicated that vesicle release remains relatively synchronous during tonic stimulation.

High-fidelity spike propagation at Schaffer collateral axons

It is conceivable that failure of axonal conduction could cause us to underestimate rates of release. To investigate whether axonal conduction was reliable (under our experimental conditions) we directly recorded extracellular potentials from single Schaffer collaterals in the CA1 area of stratum radiatum at 35°C (Raastad & Shepherd, 2003). 'Minimal stimulation' was used to elicit all-or-none responses, which were assumed to arise from single axons if increasing the stimulus intensity did not cause a significant change in response amplitude, shape or latency (Fig. 7*Aa* and *b*). With the stimulus intensity set at 25% above threshold (to compensate for activity-dependent changes in threshold) (Soleng *et al.* 2004), axons were found to fire with high fidelity during long bouts of TBS (4 stimuli at 50 Hz, presented every 200 ms). Figure 7*Ba* shows a short segment of a recording from a single fibre in response to 60 s of TBS. The peak amplitude of the action potential was stable over the course of stimulation, and showed only a few conduction failures at the beginning of the train (Fig. 7*Bb*). Although such failures were occasionally observed, on average the probability of spiking (P_{spike}) during prolonged stimulation was high (Fig. 7*C*; P_{spike} of last 100 stimuli in the train was 0.88 ± 0.01; $n = 6$). Thus, Schaffer collateral axons appear to follow high-frequency trains with high fidelity even when stimulated for prolonged periods. It is important to note that the intense stimulation protocols used here are not extreme and may represent a typical activity state of hippocampal synapses during activation by physiological stimuli (Csicsvari *et al*. 2003).

Discussion

In this study we have extended dendritic spine imaging approaches developed earlier (Muller & Connor, 1991; Murphy *et al.* 1994*a*; Yuste & Denk, 1995; Oertner *et al.*

2002) to image quantal events in dendritic spines during prolonged TBS. We have used for the first time classical fluctuation (Katz & Miledi, 1972) and deconvolution analyses of fluorescent measurements (Yaksi & Friedrich, 2006) to estimate quantal size and release rates during ongoing synaptic activity. In previous postsynaptic optical analyses of asynchronous release in cultured neurons (Otsu & Murphy, 2004), release was at a low enough rate to observe individual quanta directly. Here, in acute slices the asynchronous component was non-significant, but the relatively high release rates necessitate a deconvolution analysis. Our approach of using postsynaptic NMDA receptor activity to assess vesicular release relies on the assumption that multiple vesicles produce additive responses. But would quanta add linearly if released in quick succession? Or could the slow unbinding of glutamate from the NMDA receptors leave them in a singly bound state and cause a potentiation of responses to subsequent vesicles? A detailed previous examination of responses to paired stimuli (made with high temporal resolution) provided compelling evidence that such post-synaptic mechanisms do not significantly change the potency of a vesicle, at least when the interval between events was > 40 ms (Oertner *et al.* 2002). Thus, at steady state when we estimate the average interval between events to be $\sim$300 ms, vesicles would be expected to produce additive responses. Another potential concern with using NMDA receptors to evaluate release is that the receptors are prone to saturation (Frerking & Wilson, 1996). However, more recent elegant work from the Svoboda lab (Sobczyk *et al.* 2005) using uncaging of glutamate demonstrated that NMDA receptors are far from saturation. Furthermore, we have previously shown by rapid application of agonist to outside-out patches that NMDA receptors are expected to be far from saturation during physiological levels of release at 37°C (Chen *et al.* 2001).

Even if vesicle release could be faithfully relayed by NMDA receptors, several sources of non-linearities could be introduced during the generation and detection of Ca^{2+} signals. For example, under certain conditions Ca^{2+} release from stores can produce signals not directly associated with activity at ionotropic receptors (Emptage *et al.* 1999; Raymond & Redman, 2006). However, we used juvenile rats (< 3 weeks old) in which most spines do not contain endoplasmic reticulum (Spacek & Harris, 1997), which contrasts with another study that demonstrated Ca^{2+} release from stores in mature rats (6–8 weeks; Raymond & Redman, 2006). Furthermore, we used Cs^{+}-based intracellular solutions and whole-cell recordings that are known to block Ca^{2+} release from internal stores (Enoki & Fine, 2005). Lastly, the steady-state Ca^{2+} signal we measure was voltage dependent and linearly related to the NMDA EPSC (Figs 2 and 3). Together, these observations led us to conclude that internal stores do not contribute significantly to the TBS-evoked Ca^{2+} responses.

To alleviate non-linearities associated with the measurement of Ca^{2+} signals, we used a high concentration of calcium indicator (1 mM Fluo 5F) sacrificing optimal optical signal-to-noise. Under these conditions, the indicator constitutes the dominant buffer in the cell and severely restricts the peak synaptic Ca^{2+} concentration reached (< 400 nM; Lev-Ram *et al.* 1992). Limiting Ca^{2+} elevation is expected not only to reduce non-linearities in cellular extrusion or buffering mechanisms (Tank *et al.* 1995), but also Ca^{2+}-dependent changes in processes such as extrusion (Scheuss *et al.* 2006) and NMDA receptor desensitization (Tong *et al.* 1995) or modification (Sobczyk & Svoboda, 2007). Finally, using subsaturating concentrations of the competitive antagonist (1–5 μM AP5) we showed that NMDA-mediated Ca^{2+} signals and currents are blocked with equal efficacy (Fig. 6), confirming that non-linearities in Ca^{2+} detection did not cause a substantial distortion of our measurements. Thus, under our experimental conditions, the steady-state spine Ca^{2+} signal is expected

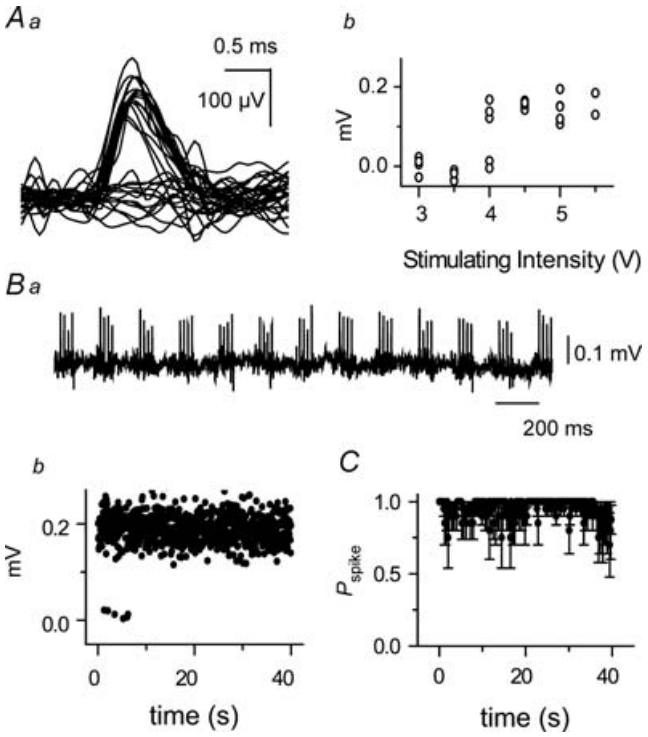

Figure 7. High-fidelity conduction at single axons in the stratum radiatum
Aa, extracellular recordings from single axons show a characteristic 'all-or-none' response to increasing stimulus intensity. *Ab*, the peak spike amplitude is plotted against stimulus intensity. *Bi*, the response of the same axon as in *A*, to prolonged TBS (bursts of 4 pulses at 50 Hz delivered every 200 ms). *Bb*, the peak spike amplitude is plotted against stimulus number. *C*, binarized responses (0 failures, 1 success) from 6 axons were averaged to compute the probability of spike conduction (P_{spike}).

to arise from a near-linear addition of events initiated by glutamate release from single vesicles.

NMDA receptor function during sustained activity

NMDA receptors are modulated by a variety of signalling pathways (Kotecha & MacDonald, 2003). However, these did not appear to play a large role in the time frame and conditions of our experiments, since depression of NMDA-mediated EPSCs during prolonged TBS roughly paralleled the decay of the peak amplitude of AMPA EPSCs. In addition, the average quantal size estimates derived from fluctuations of steady-state Ca^{2+} signal during sustained TBS were similar to those measured during LFS. The credibility of such analysis is borne out in the partial NMDA receptor antagonism experiments where the variance-to mean ratios (quantal size estimates) could be changed in predictable manner without changing the apparent release rate (Fig. 6). Thus, postsynaptic NMDA receptor-mediated Ca^{2+} transients appear to reflect vesicle rate during intense stimulation. The constant amplitude of NMDA receptor-mediated quantal responses parallels information transfer by AMPA receptors during high-frequency stimulation (Zhou *et al.* 2000). However, one caveat is that local Ca^{2+} buffering by the Ca^{2+} indicator might itself prevent modulation of NMDA receptors by processes such as desensitization, inactivation or other means of down-regulation (Tong *et al.* 1995; Morishita *et al.* 2005; Sobczyk & Svoboda, 2007). Although buffering by the Ca^{2+} indicator will affect Ca^{2+}-dependent means of receptor regulation, it helps to ensure that the fluorescent signals we measure are a faithful indicator of neurotransmitter release.

Effective release rates at Schaffer collateral to CA1 synapses

In the rat hippocampus, the Schaffer collateral axons are thin (0.17 μm), unmyelinated, highly branched and have numerous en passant boutons (Shepherd & Harris, 1998), making them potentially prone to conduction failure (Brody & Yue, 2000; Debanne, 2004). Our experiments depend on reliable stimulation to cause vesicle depletion, and thus conduction failure could be a confounding factor. However, we found that Schaffer collateral axons could follow high-frequency TBS stimuli for prolonged periods (Fig. 7). The fidelity of Schaffer collaterals are consistent with findings that hippocampal networks are capable of maintaining synchronous bursting activity at theta frequencies (5–20 Hz) for prolonged periods (Czurko *et al.* 1999) during physiological activation of these neurons.

Since the functional integrity of NMDA receptors appeared to be preserved during tonic stimulation, we interpret the plateau level of the TBS-evoked Ca^{2+} response to directly reflect the steady-state release rate profile at the synapse. Although individual vesicles within a synaptic bouton may recycle at different rates (Fernandez-Alfonso & Ryan, 2004), our measurements do not distinguish these and provide an average release rate for a given synapse. We found that the steady-state release rate varied along a continuum, with a skew towards higher release rates. Depending on the pattern of stimulation, multiple steps including different forms of vesicle exocytosis (Xu *et al.* 2002; Harata *et al.* 2006) and endocytosis (Wang & Kaczmarek, 1998; Sara *et al.* 2002; Fernandez-Alfonso & Ryan, 2004), depletion of Ca^{2+} in the synaptic cleft (Rusakov & Fine, 2003), recovery of voltage-gated Ca^{2+} channels (Xu & Wu, 2005) and/or the release sensor (Hsu *et al.* 1996) from inactivation, and the recruitment of a variety of modulatory factors (Stevens & Sullivan, 1998; Chen *et al.* 2002; Baimoukhametova *et al.* 2004; Tyler *et al.* 2006) could determine the effective vesicle replenishment rate at a synapse. Hence, the heterogeneity in the steady-state release rates we observe could arise from a variety of sources. However, regardless of the precise molecular mechanism, we find that vesicles appear to recycle at an effective rate of ~2–3 quanta s^{-1} during sustained TBS.

Using methods previously described (Wesseling & Lo, 2002), we analysed the decay and steady-state level of the peak amplitude of AMPA-mediated EPSCs evoked by train stimulation, and estimated the unitary rate of replenishment to be ~0.02 s^{-1}. This rate is significantly smaller than that reported previously by Wesseling and Lo, conceivably due to relatively complex effects of higher physiological temperature used in our present study. It may be counterintuitive that our experiments at elevated temperature show a slower unitary rate of replenishment. However, one needs to consider that release rates will depend on both the rate of recovery and the number of vesicles that are capable of release. Notably, we observe a much larger pool of recycling quanta than Wesseling and Lo (approximate area under EPSC plot minus the steady-state) at 35°C consistent with the results of others when room temperature and physiological temperature were compared (Kushmerick *et al.* 2006). A variety of factors including the rate of vesicle endocytosis (Fernandez-Alfonso & Ryan, 2004) and apparent synaptic depression (Pyott & Rosenmund, 2002) are highly dependent on temperature and could contribute to differences in pool size. In our experiments, the number of stimuli needed to drive the responses to steady state were more than an order of magnitude larger than the number of stimuli required at room temperature (Wesseling & Lo, 2002). The large number of stimuli applied here are expected to deplete the TRP of vesicles (Von Gersdorff & Matthews, 1997; Murthy & Stevens, 1999; Harata *et al.* 2001). The TRP reflects recycling vesicles that can be mobilized over the course of seconds and consists of ~20% of the total number of

vesicles at these synapses (Harata *et al.* 2001; Rizzoli & Betz, 2005). Thus, the total number of recycling vesicles corresponds to ~40–100 vesicles of the ~200–500 vesicles present at juvenile CA1 synapses. The replenishment rate we measured electrophysiologically, thus predicts that synapses would maximally release vesicles at a rate of ~0.8–2 vesicles s^{-1} (= unitary replenishment rate s^{-1} × number of recycling vesicles), which is in line with our estimates based on Ca^{2+} measurements at single synapses.

Comparison with previous studies

The apparent vesicle replenishment rate we measured during sustained activity is significantly slower than that measured during less intense activity (Pyle *et al.* 2000; Harata *et al.* 2006), which is consistent with the general finding that the endocytosis becomes prolonged as the duration of stimulation is increased (von Gersdorff & Matthews, 1997; Wesseling & Lo, 2002; Wu, 2004). The average rate we report here is similar to that estimated from direct imaging of vesicle turnover in neuronal cultures (Sankaranarayanan & Ryan, 2000; Sara *et al.* 2002). The relative agreement here was surprising since hippocampal neurons in culture can rely on an asynchronous mode of release during sustained stimulation (Otsu *et al.* 2004; Maximov & Sudhof, 2005), which may require distinct priming steps (Fesce, 1999). These findings suggest that the rate-limiting steps in the generation of release-competent vesicles may be conserved in these different preparations. It is possible that the slow kinetics of conventional clathrin-mediated endocytosis (Heuser & Reese, 1973; Granseth *et al.* 2006), or the saturation of an endocytotic step with limited capacity (Sankaranarayanan & Ryan, 2000) limits synaptic transfer at these synapses during prolonged stimulation.

Conclusions

Based on single synapse imaging during TBS, we suggest that vesicle cycling and not postsynaptic receptor properties limit information transfer at small cortical synapses.

When Schaffer collaterals are stimulated at 20 Hz, local synapse-specific postsynaptic Ca^{2+} signalling would only be initiated at an average of ~2–3 Hz. Thus, release of a vesicle is transformed into a spatially restricted Ca^{2+} domain within each postsynaptic element (the size of domain is overestimated here due to distortion by the Ca^{2+} indicator). The heterogeneity in release rates between inputs impinging on CA1 neurons predict that similar patterns of presynaptic action potentials would trigger different forms of synaptic plasticity at individual synapses. Perhaps local biochemical effectors such as CaM kinase II (Murphy *et al.* 1994*b*; Lisman *et al.* 1997; Holmes, 2000) could be tuned to unique frequencies of postsynaptic activity triggered by synapse-specific differences in steady-state release.

References

Abbott LF, Varela JA, Sen K & Nelson SB (1997). Synaptic depression and cortical gain control. *Science* **275**, 220–224.

Baimoukhametova DV, Hewitt SA, Sank CA & Bains JS (2004). Dopamine modulates use-dependent plasticity of inhibitory synapses. *J Neurosci* **24**, 5162–5171.

Brody DL & Yue DT (2000). Release-independent short-term synaptic depression in cultured hippocampal neurons. *J Neurosci* **20**, 2480–2494.

Chen N, Ren J, Raymond LA & Murphy TH (2001). Changes in agonist concentration dependence that are a function of duration of exposure suggest N-methyl-D-aspartate receptor nonsaturation during synaptic stimulation. *Mol Pharmacol* **59**, 212–219.

Chen S, Zheng X, Schulze KL, Morris T, Bellen H & Stanley EF (2002). Enhancement of presynaptic calcium current by cysteine string protein. *J Physiol* **538**, 383–389.

Csicsvari J, Jamieson B, Wise KD & Buzsaki G (2003). Mechanisms of gamma oscillations in the hippocampus of the behaving rat. *Neuron* **37**, 311–322.

Czurko A, Hirase H, Csicsvari J & Buzsaki G (1999). Sustained activation of hippocampal pyramidal cells by 'space clamping' in a running wheel. *Eur J Neurosci* **11**, 344–352.

Debanne D (2004). Information processing in the axon. *Nat Rev Neurosci* **5**, 304–316.

Diamond JS & Jahr CE (1995). Asynchronous release of synaptic vesicles determines the time course of the AMPA receptor-mediated EPSC. *Neuron* **15**, 1097–1107.

Dudek SM & Bear MF (1992). Homosynaptic long-term depression in area CA1 of hippocampus and effects of N-methyl-D-aspartate receptor blockade. *Proc Natl Acad Sci U S A* **89**, 4363–4367.

Elmqvist D & Quastel DM (1965). A quantitative study of end-plate potentials in isolated human muscle. *J Physiol* **178**, 505–529.

Emptage N, Bliss TV & Fine A (1999). Single synaptic events evoke NMDA receptor-mediated release of calcium from internal stores in hippocampal dendritic spines. *Neuron* **22**, 115–124.

Enoki R & Fine A (2005). Ryanodine receptors and internal stores are the source of synaptic calcium transients in dendritic spines but are inactivated by patch recording. *Abstr Soc Neurosci* 968.14.

Fernandez-Alfonso T & Ryan TA (2004). The kinetics of synaptic vesicle pool depletion at CNS synaptic terminals. *Neuron* **41**, 943–953.

Fesce R (1999). The kinetics of nerve-evoked quantal secretion. *Philos Trans R Soc Lond B Biol Sci* **354**, 319–329.

Frerking M & Wilson M (1996). Saturation of postsynaptic receptors at central synapses? *Curr Opin Neurobiol* **6**, 395–403.

Granseth B, Odermatt B, Royle SJ & Lagnado L (2006). Clathrin-mediated endocytosis is the dominant mechanism of vesicle retrieval at hippocampal synapses. *Neuron* **51**, 773–786.

Haller M, Heinemann C, Chow RH, Heidelberger R & Neher E (1998). Comparison of secretory responses as measured by membrane capacitance and by amperometry. *Biophys J* **74**, 2100–2113.

Hanse E & Gustafsson B (2001). Paired-pulse plasticity at the single release site level: an experimental and computational study. *J Neurosci* **21**, 8362–8369.

Harata NC, Choi S, Pyle JL, Aravanis AM & Tsien RW (2006). Frequency-dependent kinetics and prevalence of kiss-and-run and reuse at hippocampal synapses studied with novel quenching methods. *Neuron* **49**, 243–256.

Harata N, Pyle JL, Aravanis AM, Mozhayeva M, Kavalali ET & Tsien RW (2001). Limited numbers of recycling vesicles in small CNS nerve terminals: implications for neural signaling and vesicular cycling. *Trends Neurosci* **24**, 637–643.

Heuser JE & Reese TS (1973). Evidence for recycling of synaptic vesicle membrane during transmitter release at the frog neuromuscular junction. *J Cell Biol* **57**, 315–344.

Holmes WR (2000). Models of calmodulin trapping and CaM kinase II activation in a dendritic spine. *J Comput Neurosci* **8**, 65–85.

Hsu SF, Augustine GJ & Jackson MB (1996). Adaptation of Ca^{2+} -triggered exocytosis in presynaptic terminals. *Neuron* **17**, 501–512.

Katz B & Miledi R (1972). The statistical nature of the acetycholine potential and its molecular components. *J Physiol* **224**, 665–699.

Kotecha SA & MacDonald JF (2003). Signaling molecules and receptor transduction cascades that regulate NMDA receptor-mediated synaptic transmission. *Int Rev Neurobiol* **54**, 51–106.

Kushmerick C, Renden R & Von Gersdorff H (2006). Physiological temperatures reduce the rate of vesicle pool depletion and short-term depression via an acceleration of vesicle recruitment. *J Neurosci* **26**, 1366–1377.

Lev-Ram V, Miyakawa H, Lasser-Ross N & Ross WN (1992). Calcium transients in cerebellar Purkinje neurons evoked by intracellular stimulation. *J Neurophysiol* **68**, 1167–1177.

Lisman J, Malenka RC, Nicoll RA & Malinow R (1997). Learning mechanisms: the case for CaM-KII. *Science* **276**, 2001–2002.

Maximov A & Sudhof TC (2005). Autonomous function of synaptotagmin 1 in triggering synchronous release independent of asynchronous release. *Neuron* **48**, 547–554.

Morishita W, Marie H & Malenka RC (2005). Distinct triggering and expression mechanisms underlie LTD of AMPA and NMDA synaptic responses. *Nat Neurosci* **8**, 1043–1050.

Muller W & Connor JA (1991). Dendritic spines as individual neuronal compartments for synaptic Ca^{2+} responses. *Nature* **354**, 73–76.

Murphy TH, Baraban JM, Wier WG & Blatter LA (1994*a*). Visualization of quantal synaptic transmission by dendritic calcium imaging. *Science* **263**, 529–532.

Murphy TH, Blatter LA, Bhat RV, Fiore RS, Wier WG & Baraban JM (1994*b*). Differential regulation of calcium/calmodulin-dependent protein kinase II and p42 MAP kinase activity by synaptic transmission. *J Neurosci* **14**, 1320–1331.

Murthy VN, Sejnowski TJ & Stevens CF (1997). Heterogeneous release properties of visualized individual hippocampal synapses. *Neuron* **18**, 599–612.

Murthy VN & Stevens CF (1999). Reversal of synaptic vesicle docking at central synapses. *Nat Neurosci* **2**, 503–507.

Oertner TG, Sabatini BL, Nimchinsky EA & Svoboda K (2002). Facilitation at single synapses probed with optical quantal analysis. *Nat Neurosci* **5**, 657–664.

Otsu Y & Murphy TH (2004). Optical postsynaptic measurement of vesicle release rates for hippocampal synapses undergoing asynchronous release during train stimulation. *J Neurosci* **24**, 9076–9086.

Otsu Y, Shahrezaei V, Li B, Raymond LA, Delaney KR & Murphy TH (2004). Competition between phasic and asynchronous release for recovered synaptic vesicles at developing hippocampal autaptic synapses. *J Neurosci* **24**, 420–433.

Prange O & Murphy TH (1999). Analysis of multiquantal transmitter release from single cultured cortical neuron terminals. *J Neurophysiol* **81**, 1810–1817.

Pyle JL, Kavalali ET, Piedras-Renteria ES & Tsien RW (2000). Rapid reuse of readily releasable pool vesicles at hippocampal synapses. *Neuron* **28**, 221–231.

Pyott SJ & Rosenmund C (2002). The effects of temperature on vesicular supply and release in autaptic cultures of rat and mouse hippocampal neurons. *J Physiol* **539**, 523–535.

Raastad M & Shepherd GM (2003). Single-axon action potentials in the rat hippocampal cortex. *J Physiol* **548**, 745–752.

Raymond CR & Redman SJ (2006). Spatial segregation of neuronal calcium signals encodes different forms of LTP in rat hippocampus. *J Physiol* **570**, 97–111.

Rizzoli SO & Betz WJ (2005). Synaptic vesicle pools. *Nat Rev Neurosci* **6**, 57–69.

Rosenmund C, Sigler A, Augustin I, Reim K, Brose N & Rhee JS (2002). Differential control of vesicle priming and short-term plasticity by Munc13 isoforms. *Neuron* **33**, 411–424.

Rusakov DA & Fine A (2003). Extracellular Ca^{2+} depletion contributes to fast activity-dependent modulation of synaptic transmission in the brain. *Neuron* **37**, 287–297.

Sabatini BL, Oertner TG & Svoboda K (2002). The life cycle of Ca^{2+} ions in dendritic spines. *Neuron* **33**, 439–452.

Sankaranarayanan S & Ryan TA (2000). Real-time measurements of vesicle-SNARE recycling in synapses of the central nervous system. *Nat Cell Biol* **2**, 197–204.

Sara Y, Mozhayeva MG, Liu X & Kavalali ET (2002). Fast vesicle recycling supports neurotransmission during sustained stimulation at hippocampal synapses. *J Neurosci* **22**, 1608–1617.

Scheuss V, Yasuda R, Sobczyk A & Svoboda K (2006). Nonlinear $[Ca^{2+}]$ signaling in dendrites and spines caused by activity-dependent depression of Ca^{2+} extrusion. *J Neurosci* **26**, 8183–8194.

Shepherd GM & Harris KM (1998). Three-dimensional structure and composition of CA3 →CA1 axons in rat hippocampal slices: implications for presynaptic connectivity and compartmentalization. *J Neurosci* **18**, 8300–8310.

Sobczyk A, Scheuss V & Svoboda K (2005). NMDA receptor subunit-dependent $[Ca^{2+}]$ signaling in individual hippocampal dendritic spines. *J Neurosci* **25**, 6037–6046.

Sobczyk A & Svoboda K (2007). Activity-dependent plasticity of the NMDA-receptor fractional Ca^{2+} current. *Neuron* **53**, 17–24.

Soleng AF, Baginskas A, Andersen P & Raastad M (2004). Activity-dependent excitability changes in hippocampal CA3 cell Schaffer axons. *J Physiol* **560**, 491–503.

Spacek J & Harris KM (1997). Three-dimensional organization of smooth endoplasmic reticulum in hippocampal CA1 dendrites and dendritic spines of the immature and mature rat. *J Neurosci* **17**, 190–203.

Stevens CF & Sullivan JM (1998). Regulation of the readily releasable vesicle pool by protein kinase C. *Neuron* **21**, 885–893.

Stevens CF & Wang Y (1995). Facilitation and depression at single central synapses. *Neuron* **14**, 795–802.

Tank DW, Regehr WG & Delaney KR (1995). A quantitative analysis of presynaptic calcium dynamics that contribute to short-term enhancement. *J Neurosci* **15**, 7940–7952.

Tong G, Shepherd D & Jahr CE (1995). Synaptic desensitization of NMDA receptors by calcineurin. *Science* **267**, 1510–1512.

Tyler WJ, Zhang XL, Hartman K, Winterer J, Muller W, Stanton PK & Pozzo-Miller L (2006). BDNF increases release probability and the size of a rapidly recycling vesicle pool within rat hippocampal excitatory synapses. *J Physiol* **574**, 787–803.

Van der Kloot W (1988). Estimating the timing of quantal releases during end-plate currents at the frog neuromuscular junction. *J Physiol* **402**, 595–603.

Von Gersdorff H & Matthews G (1997). Depletion and replenishment of vesicle pools at a ribbon-type synaptic terminal. *J Neurosci* **17**, 1919–1927.

Wadiche JI & Jahr CE (2001). Multivesicular release at climbing fiber-Purkinje cell synapses. *Neuron* **32**, 301–313.

Wang LY & Kaczmarek LK (1998). High-frequency firing helps replenish the readily releasable pool of synaptic vesicles. *Nature* **394**, 384–388.

Wesseling JF & Lo DC (2002). Limit on the role of activity in controlling the release-ready supply of synaptic vesicles. *J Neurosci* **22**, 9708–9720.

Wu LG (2004). Kinetic regulation of vesicle endocytosis at synapses. *Trends Neurosci* **27**, 548–554.

Xu J & Wu LG (2005). The decrease in the presynaptic calcium current is a major cause of short-term depression at a calyx-type synapse. *Neuron* **46**, 633–645.

Xu J, Xu Y, Ellis-Davies GC, Augustine GJ & Tse FW (2002). Differential regulation of exocytosis by α- and β-SNAPs. *J Neurosci* **22**, 53–61.

Yaksi E & Friedrich RW (2006). Reconstruction of firing rate changes across neuronal populations by temporally deconvolved Ca^{2+} imaging. *Nat Meth* **3**, 377–383.

Yuste R & Denk W (1995). Dendritic spines as basic functional units of neuronal integration. *Nature* **375**, 682–684.

Zhou Q, Petersen CC & Nicoll RA (2000). Effects of reduced vesicular filling on synaptic transmission in rat hippocampal neurones. *J Physiol* **525**, 195–206.

Acknowledgements

This work was supported by a CIHR operating grant to T.H.M., MOP 12675 and MOP 14455 to K.R.D. We thank Dr H. Taschenberger (Gottingen, Germany) for help with programming, Dr J. Wesseling (Pamplona, Spain) for his helpful comments on modelling synaptic depression, Alexander Goroshkov for his technical assistance, and Drs Thomas Oertner and Craig Brown for their critical comments on the manuscript.

Supplemental material

Online supplemental material for this paper can be accessed at:
http://jp.physoc.org/cgi/content/full/jphysiol.2007.130286/DC1
and
http://www.blackwell-synergy.com/doi/suppl/10.1113/jphysiol.2007.130286

Effective release rates at single rat Schaffer collateral–CA1 synapses during sustained theta-burst activity revealed by optical imaging

G. B. Awatramani, J. D. Boyd, K. R. Delaney and T. H. Murphy

J. Physiol. 2007;582;583-595; originally published online Apr 26, 2007;

DOI: 10.1113/jphysiol.2007.130286

Supplementary Figure

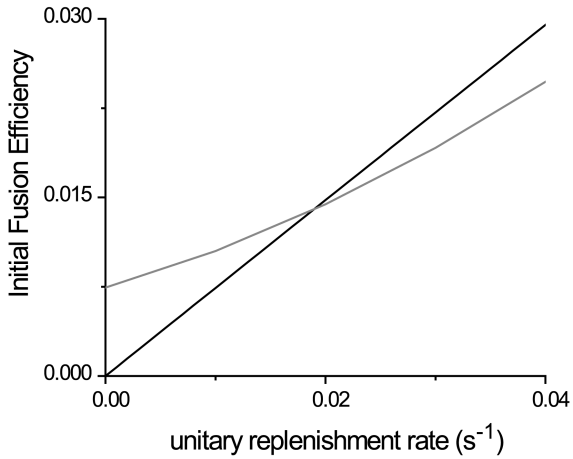

Awatramani et al. Supplementary Fig.

Supplementary Information Awatramani et al.

Estimating the replenishment rate constant (α) from EPSC evoked by train stimuli

Since some fraction of the response recovers during the train, the sum of the responses evoked by the first 900 stimuli provides an overestimate of the capacity of the TRP. Assuming that the average steady-state response is proportional to the amount recovered during the interstimulus interval (Wesseling & Lo, 2002), dividing it by the sum of the responses evoked by the first 900 stimuli yields the fraction of TRP that recovered during the time between stimuli (estimated to be 0.0006 of the TRP). Since 20 stimuli were applied every second, this translates into a rate of 0.012/s (0.0006*20) and represents a lower bound for the estimate of α, the replenishment rate. On the other hand, if the amount of replenishment during the first 45 s is assumed to be similar to that at the end of the train, then the estimated TRP would be smaller by an amount approximated by the amount of steady state release observed at the end of the train (~55% of the initial response could be accounted for by vesicles recovered during the train). Excluding this recovered fraction yields an overestimate for the rate for TRP recovery of 0.027/s. However, the actual rate of replenishment of the TRP should therefore fall somewhere between these two estimates.

To estimate the true replenishment rate more accurately (within the limits stated above) during continuous stimulation we followed methods previously described by Wesseling and Lo (Wesseling & Lo, 2002). The simple kinetic model can be formally stated as:

$$\frac{dn}{dt} \quad \alpha \cdot (N-n) - \beta \cdot n \qquad \text{Equation S1}$$

where α represents the replenishment rate constant, β the unitary rate of exocytosis, n the number of vesicles available for release, and N is the total number of vesicles in the TRP. This model is similar to that used for evaluating the kinetics of recovery of the readily releasable pool of vesicles (Stevens & Wang, 1995; Wesseling & Lo, 2002). When the pool is in a depleted state and there is no exocytosis (β=0), then the pool recovers exponentially. At steady state, the amount of recovery can be estimated by the amount of exocytosis triggered by each stimulus r(∞):

$$r(\infty) = N \cdot (1-e^{-\alpha/\nu})$$

where ν is the frequency of stimulation. Since N is difficult to estimate (because the number of fibers stimulated is not known), the initial fusion efficiency (f_e) defined as the fraction of the TRP released by the first stimulus (f_e = r(1)/N), is a more convenient parameter. Substituting f_e into the above equation:

$$f_e = \frac{r(1)}{r(\infty)} \quad -e^{-\alpha/\nu}) \qquad \text{Equation S2}$$

This equation describes the relationship between f_e and α and is plotted as a solid black line in Supplementary Figure 1.

A second independent equation relating f_e and α can be derived from equation S1, that in contrast depends more on the initial responses to the high frequency train. The true capacity of the TRP can be estimated as:

$$N = \sum_{i=1}^{S} \quad) - w(S)$$

Where w(S) is the fraction of the response that recovers and subsequently undergoes depression during the long train. w(S) can be estimated as (Wesseling and Lo, 2002):

$$w(S) = \sum_{i=1}^{S} \quad i) \cdot (1-e^{-\alpha \cdot (S-i)/v}) \qquad \text{Equation S3}$$

Combining the above two equations and expressing N in terms of *fe*:

$$f_e = - \frac{r(1)}{\sum_{i=1}^{S} r(i) \cdot e^{-\alpha \cdot (S-i)/v}} \qquad \text{Equation S4}$$

Equation S4 is plotted as the gray line in Supplementary Figure 1. Equation S2 and S4 are independent as they rely on the steady state and the initial responses, respectively. These equations are most easily solved numerically (Supplementary Figure 1), and for our data set we calculate an average α of ~0.02/s. A more extensive treatment of these equations and a verification of the assumptions underlying them can be found elsewhere (Wesseling & Lo, 2002).